Voltage Distribution Modeling Along Stator Windings in Permanent Magnet Synchronous Machines Using Coil-Based Grey Box Models

Hujun Peng, Svetomir Stevic, *Graduate Student Member, IEEE*, Ze Luo, Niklas Driendl, Daniel Butterweck, Leila Sharifian, Yousef Firouz, and Kay Hameyer, *Senior Member, IEEE*

***Abstract*—A coil-based grey box model is developed for high-frequency modeling of permanent magnet synchronous machines (PMSMs) with interior magnets in rotors to predict the voltage distribution along stator winding. Unlike the grey box model in the literature, the developed coil-based model can predict the voltage distribution along stator winding. Compared to the white box model, no complex modeling based on finite element simulation results is required. As the name suggests, the developed model has each winding coil as a basis, and the entire model is created by connecting coils according to the winding schema. Furthermore, the coil-based model considers frequency-dependent inductive and capacitive coupling within electrical machines, including skin and proximity effects. The model is parametrized using an optimization program based on measured impedance spectra at machine terminals. As a result, an average deviation of less than 4 % is observed in the impedance modeling. With the coil-based model's help, the common mode voltage distribution is predicted with almost zero errors between modeled and measured voltage peak values. Regarding the differential mode voltage distribution, the voltage maximum can be predicted with a maximum relative error of less than 10 % in the time domain.**

***Index Terms*—Converter machine interactions, electrical drive, high-frequency windings, grey box model, permanent magnet machines, voltage distribution prediction.**

I. Introduction

HAIRPIN windings are increasingly utilized in automotive applications due to their significantly higher copper fill factor compared to round conductors [1]. Moreover, reducing hairpin windings' insulation thickness is desirable to enhance further the copper fill factor and power density of electrical motors. In addition to hairpin windings, automotive applications increasingly employ semiconductor modules such as SiC and GaN. These materials offer advantages such as low switching losses, high switching frequency, and high-temperature endurance. However, the fast switching of these semiconductor power modules leads to high voltage slew rates, which can induce voltage oscillation behavior in electrical machines [2], [3]. These voltage oscillations occur due to the interaction among inverters, cables, and electrical machines [4]. To address this issue, motor designers can adjust the configuration of the insulation system based on the maximum electrical stress in the electrical machines, given the knowledge of voltage peaks and their oscillation frequency [5].

Existing literature indicates that the maximum voltage in electrical machines can reach twice the DC-link voltage due to the impedance mismatch between cables and electrical machines [6], [7]. Consequently, in practical applications, insulation layers are often overdesigned to avoid partial discharge in electrical machines. It becomes necessary to predict the maximum peak voltage within the electrical machines to avoid insulation overdesign [8], [9]. Then, the insulation system of electrical machines can be designed with minimal thickness while ensuring the absence of partial discharge phenomena [10], [11]. Accurate high-frequency modeling of electrical machines is crucial for calculating the maximum voltage stress [12].

The high-frequency models include two main types: the grey box model and the white box model. The grey box modeling method analyzes the external interactions of electrical machines with cables and inverters. In the grey box model, electrical circuits with lumped parameters are proposed. The parameters of the grey box model are determined by fitting the measured impedance spectra at machine terminals. The grey box models have been well-developed for induction machines in [13] and surface-mounted PMSM in [14]. In [15], [16], the mutual inductance among different coils of electrical machines is realized using an invariant value. Nevertheless, the implementation of frequency-dependent mutual inductances is not finished. Besides that, the grey box model for the PMSM with internal permanent magnets in rotors is not seen in the literature. It is acknowledged that the asymmetry between the d and q axes brings more complexity for modeling than induction motors and surface-mounted PMSM. Overall, the classical grey box model found in the literature cannot predict electrical potential distribution within the electrical machines. In order

Manuscript received 6 September 2023; revised 13 November 2023, 26 December 2023, and 24 February 2024; accepted 24 February 2024. Date of publication 27 February 2024; date of current version 22 August 2024. This work was supported by Toyota Motor Corporation. Paper no. TEC-01023-2023. *(Corresponding author: Hujun Peng.)*

Hujun Peng, Svetomir Stevic, Ze Luo, Niklas Driendl, Daniel Butterweck, and Kay Hameyer are with the Institute of Electrical Machines (IEM), RWTH Aachen University, 52062 Aachen, Germany.

Leila Sharifian and Yousef Firouz are with the Toyota Motor Europe 1930, Belgium.

Color versions of one or more figures in this article are available at https://doi.org/10.1109/TEC.2024.3370800.

Digital Object Identifier 10.1109/TEC.2024.3370800

to address this limitation, the so-called white-box model is applied [17].

The white-box model utilizes the FEM to parameterize the equivalent electrical circuit. It is more complex compared to the grey box model [18], [19]. In [20], the frequency-dependent mutual impedance among neighboring conductors is implemented using current-controlled voltage sources, representing state-of-the-art white box modeling. It should be noted that in [20], the mutual impedance is implemented independently from the self-impedance. Such an implementation of mutual inductances significantly increases the number of fitting parameters, not reflecting practical considerations. Overall, the white-box model is complicated and time-consuming, making it challenging to implement [21].

The literature review shows that no research has proposed a grey box model capable of predicting electrical potential distribution along the stator winding using impedance measurement data. Furthermore, modeling PMSMs with V-shape interior permanent magnets is more complicated than surface-mounted PMSMs or induction motors. Consequently, this work aims to address the gaps mentioned above. The following contributions are presented:

- A coil-based model is developed for PMSMs to predict the voltage distribution along the stator winding with the minimum effort of measuring impedance at machine outer terminals.
- The developed model helps to determine the voltage differences that are most critical for the design of the electrical machine's internal insulation. The developed model has a winding coil as the element, which shows the accuracy of the voltage distribution determination at the coil level. The resolution achieved is sufficient since the coil-based model can identify the electric stress at the most crucial point.
- Compared to existing works, frequency-dependent mutual inductances are also considered, besides the self-inductances.
- The coil-based model shows an averaged deviation of less than 4 % in the frequency domain up to 2 MHz. More importantly, all primary resonance points are accurately modeled in common and differential mode impedance spectra.
- Test bench measurements are carried out to validate the accuracy of the developed model in predicting the voltage distribution along stator windings. No other research works have been found to validate similiar high-frequency models on an operational electrical machine.

The structure of the paper is as follows: Section II presents the measurement configuration and motor adjustments required for voltage measurement within the motors. Section III proposes the coil-based grey box model, considering inductive and capacitive coupling among coils of the same and different phases. Section IV validates the model in the frequency domain by comparing the modeled impedance spectra with measured values for different topologies. Section V demonstrates the validation results of the coil-based grey box model in the time domain based on test bench measurements. Finally, Section VI concludes the paper and provides future perspectives.

TABLE I
DISTRIBUTION OF THE VOLTAGE MEASURING POINTS WITHIN THE ELECTRICAL MACHINE, WHEREBY EACH PHASE HAS 16 COILS CONNECTED IN SERIALS WITH EACH COIL CONSISTING OF 8 CONDUCTORS

Symbol	Meaning
U1e	Welding point after the 10-th conductor in 2-nd U-coil
U7e	Welding point after the 58-th conductor in 8-th U-coil
U8e	Welding point after the 66-th conductor in 9-th U-coil
U9e	Welding point after the 74-th conductor in 10-th U-coil
V1e	Welding point after the 10-th conductor in 2-nd V-coil
V7e	Welding point after the 58-th conductor in 8-th V-coil
V8e	Welding point after the 66-th conductor in 9-th V-coil
V9e	Welding point after the 74-th conductor in 10-th V-coil
W1e	Welding point after the 10-th conductor in 2-nd W-coil
W7e	Welding point after the 58-th conductor in 8-th W-coil
W8e	Welding point after the 66-th conductor in 9-th W-coil
W9e	Welding point after the 74-th conductor in 10-th W-coil

II. Setup of Measuring Impedance Spectra of the PMSM and Its Results

This section introduces the impedance spectra of the PMSM to be modeled, including various connection topologies during measuring. The internal welding points, which will be later used to validate the model in predicting voltage distribution along stator windings, are also introduced.

The PMSM provided by Toyota has a pole pair number of four, and the slot number is 48. There are eight conductors in each slot, and each phase's conductors are connected in serials. Therefore, each phase has 128 conductors connected in serials. Eight conductors in serials form a coil, and then, each phase consists of 16 coils connected in serials.

The stator winding of the electric motor has been modified to enable voltage distribution measurement along the stator windings. This modification involves attaching additional supply lines to the welding points in the hairpin windings. The supply lines for voltage measurement are labeled, and the locations of some measuring points are explained in Table I. In order to avoid insulation failure after the modification of the motor winding, extra resin materials are applied in the end winding area. The location of U9e corresponds to the 74th conductor, which exceeds the midpoint of the U-phase winding. It is important to note that the additional access points for voltage measurement within the electric machine are solely used to validate the voltage distribution modeling on the test bench in the time domain. These access points are not utilized for parameterizing the coil-based model because they are not accessible in a regular electric machine without any winding modifications. This study aims to parameterize the coil-based grey box model based on impedance spectrum measurements obtained from the motor terminals. This model is capable of predicting the voltage distribution along the stator winding.

The impedance spectrum is measured using the impedance analyzer "Keysight E4990 A", covering a frequency range from 100 Hz to 10 MHz. Different terminal motor configurations are employed during impedance measurements, as summarized in Table II and illustrated in Fig. 1. These configurations include setups of phase-to-NP, phase-to-GND, phase-to-phase, and phase-to-phases. In this context, "NP" refers to the neutral

TABLE II
MOTOR TERMINAL CONFIGURATION TOPOLOGIES FOR IMPEDANCE SPECTRUM MEASUREMENT

Symbol	Meaning
U-NP	Impedance measurement between U and NP
V-NP	Impedance measurement between V and NP
W-NP	Impedance measurement between W and NP
U-GND	Impedance measurement between U and GND
V-GND	Impedance measurement between V and GND
W-GND	Impedance measurement between W and GND
U-V	Impedance measurement between U and V
V-W	Impedance measurement between V and W
W-U	Impedance measurement between W and U
U-VW	Impedance measurement between U and VW
V-WU	Impedance measurement between V and WU
W-UV	Impedance measurement between W and UV

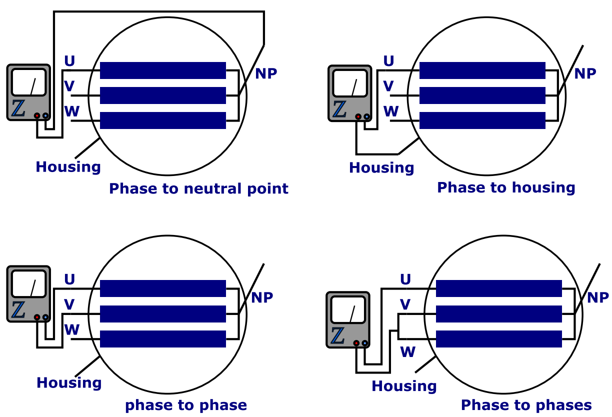

Fig. 1. Motor terminal configuration types for measuring impedance spectra.

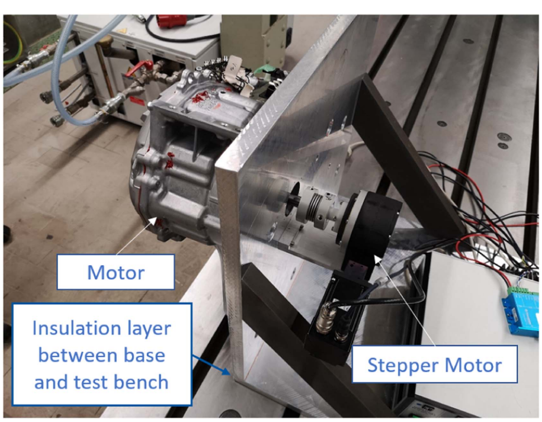

Fig. 2. Setup of the PMSM for impedance measurement.

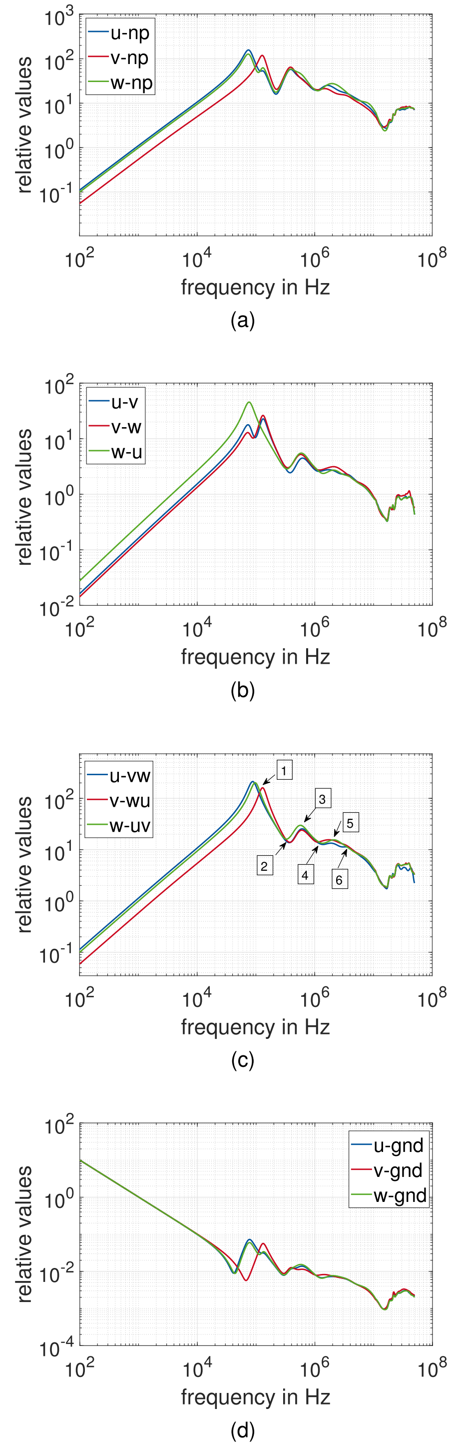

Fig. 3. Impedance spectra of different measurement configuration setups: (a) Phase-to-NP, (b) Phase-to-phase, (c) Phase-to-phases, and (d) Phase-to-housing.

point, "GND" represents the motor housing, and "VW" indicates a short-circuit connection between terminals V and W. Since the model to be developed is for the PMSM with interior magnets in rotors, measurements are conducted for all three phases due to the inherent asymmetry between phases. In order to provide accurate impedance measurement of the PMSM, a plastic layer is inserted between the test bench and the motor fixture, as shown in Fig. 2. This insulation layer is necessary as direct contact between the PMSM and the test bench can distort the measured impedance spectra.

The impedance spectra for various terminal configuration topologies are presented in Fig. 3, including phase-to-NP in Fig. 3(a), phase-to-phase in Fig. 3(b), phase-to-phases in Fig. 3(c), and phase-to-GND in Fig. 3(d). At lower frequencies, the measured impedance spectra for differential-mode terminal connections in Fig. 3(a)–(c) exhibit significant differences in amplitude. These differences result from due to the

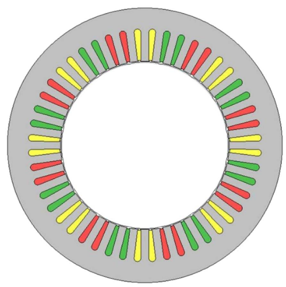

Fig. 4. Schematic slot distribution of the stator winding.

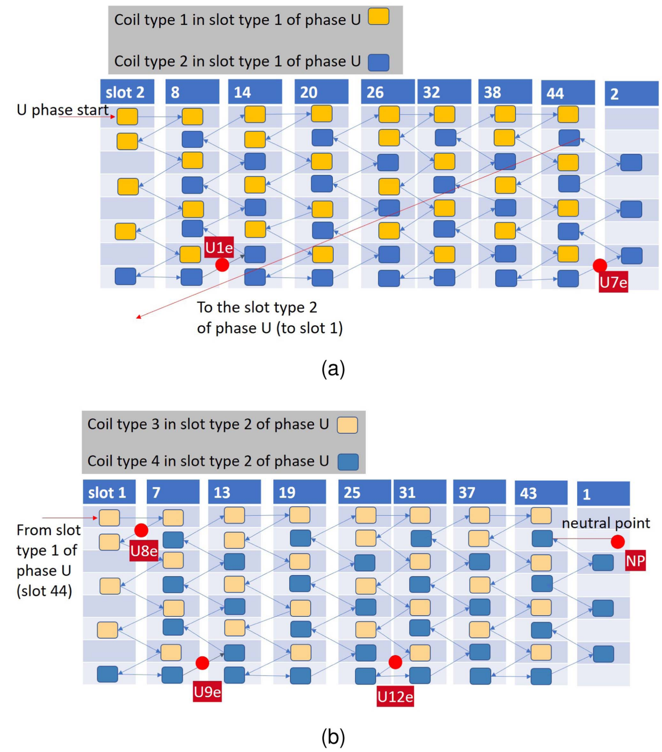

Fig. 5. Coil types in phase U: (a) Type 1 and 2 coils consisting of conductors in the type 1 slots of phase U and (b) Type 3 and 4 coils consisting of conductors in the type 2 slots of phase U.

asymmetry between the d and q axes in the PMSM. However, above 350 kHz, the impedance spectra of different phases overlap to a large extent because the asymmetry decreases with higher frequencies. Therefore, in developing a coil-based grey box model for voltage distribution modeling within the PMSM, it is essential to consider both the deviation at low frequencies and the similarity at high frequencies between phases during the parameterization process. Furthermore, six primary resonance points below 5 MHz in the impedance spectra are marked in Fig. 3(c), representing a target for the coil-based model to be developed.

III. Coil-Based Grey Box Models of the PMSM

This section introduces the principles behind the coil-based model. First, the overall structure of the coil-based model is introduced. Then, the details of each sub-system are introduced, including modeling of skin effects in each coil, modeling of proximity effect between coils of the same phase, modeling of the common mode path of each winding coil, modeling of mutual inductance between winding coils of different phases, capacitive coupling in the slot parts, capacitive coupling in the end winding areas.

A. Principles Behind the Coil-Based Model of the PMSM

Fig. 4 presents the winding schema of the entire electrical machine, whereby different color represents different phases. There are 48 slots and eight poles, meaning that the number of slots per phase per pole is two. Therefore, there are two types of slots for each phase. Each slot has eight conductors, and there are 128 conductors per phase. The winding pitch, which is the number of slots spanned by each coil in the stator winding, is six, as shown in Fig. 5(a) and (b). In Fig. 5(a), eight conductors in slot type 1 form the type 1 coil marked in deep yellow, while the subsequent eight conductors form the type 2 coil in deep blue. All conductors of types 1 and 2 coils lie in the electromagnetic equivalent slots because the winding pitch is the same as the pole pitch. The type 1 and 2 coils are serially connected alternatively before going to the second type slot of phase U. In Fig. 5(b), the types 3 and 4 coils of U phases in its second type slots are displayed, marked in light yellow and blue, respectively. Furthermore, the location of voltage measuring points along the phase U winding is also presented In Fig. 5.

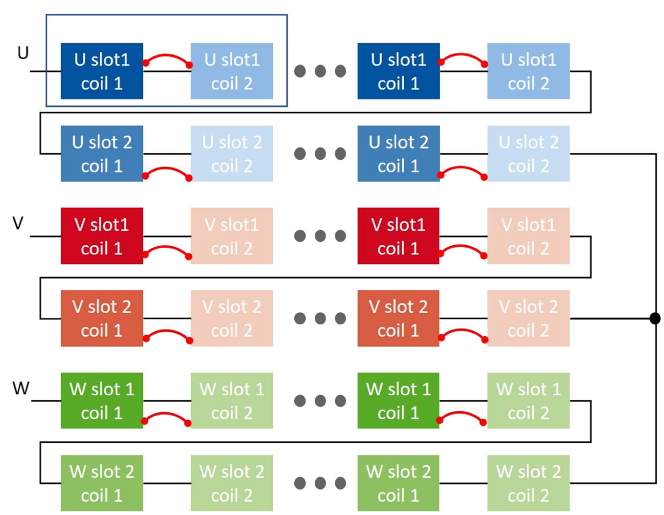

Fig. 6. Schematic presentation of mutual inductances between two subsequent coils of the same phase, whereby each phase has 16 coils connected in serials.

For each phase, two coils connected in serials have part of conductors in the same slot. Therefore, the coil-based grey box model must consider the mutual inductance between these two subsequent coils, as shown in Fig. 6. In addition, the capacitive coupling between the subsequent coils has to be modeled. Besides the coupling among coils in the slot part, the capacitive coupling in the end winding area must also be considered because the distance among conductors in the end winding area

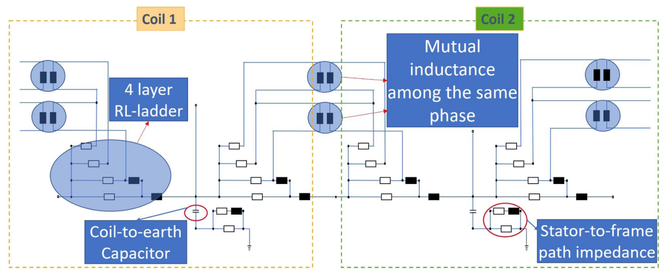

Fig. 7. Electrical circuits to consider the mutual inductances between two subsequent coils of the same phase, whereby the solid rectangular box in black represents inductance, and the hollow rectangular box represents resistance.

is also tiny. The following parts will develop a coil-based grey box model, considering these crucial inductive and capacitive coupling aspects.

B. Modeling of the Skin Effect in the Winding Coils

Each coil is modeled using a T-shape electrical circuit as shown in Fig. 7, whereby the left and right circuits are assumed to be the same to reduce the number of fitting parameters. The differential mode circuit of the coil is represented by using a four-layer RL ladder network to consider the frequency-dependent skin effects.

C. Modeling of the Proximity Effect Between Winding Coils of the Same Phase

Compared to other studies, mutual inductances are introduced to couple the two subsequent coils' first and second RL layers. It is worth mentioning that the first layer determines the inductive behaviors of the coils in the lowest-frequency range and the fourth layer for the highest-frequency range. It is assumed that the inductive coupling between two subsequent coils is more potent at low than at high frequencies. Therefore, the first and second layers of the ladder network integrate mutual inductors. In contrast, the third and fourth layer uses ordinary inductors, which considers merely skin effects instead of proximity effects between coils. The number of the RL layers can be adjusted for better fitting performance, and the actual four layers are a good choice after testing.

D. Modeling of the Common Mode Impedance of Winding Coils

The common mode path consists of a capacitor and a two-layer resistor-inductor (RL) ladder network. The capacitor represents the insulation system between the copper conductors of the coil and the stator iron. The two-layer RL ladder network considers the resistance and inductance through the stator york, which also suffers from skin effects. The capacitor is mainly determined based on the common mode impedance spectra such as U-GND. The remaining components in the two-layer RL ladder network are fitted using optimization algorithms. The ranges of the corresponding optimizing parameters are chosen based on the common mode impedance measurement results.

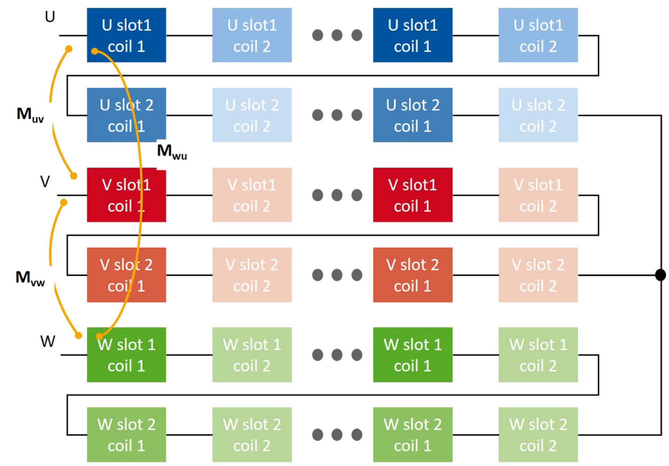

Fig. 8. Schematic presentation of mutual inductances among different phases.

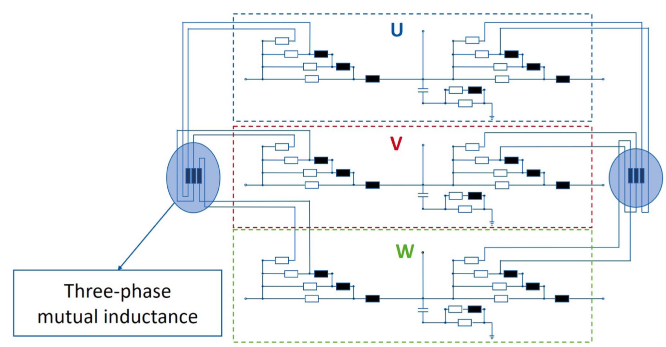

Fig. 9. Electrical circuits to consider the three-phase mutual inductance among different phases.

E. Modeling of the Proximity Effect Between Winding Coils of Different Phases

Besides the inductive coupling between subsequent coils of the same phase, there is also inductive coupling among coils of different phases in electrical machines, as shown in Fig. 8. It is assumed that the inductive coupling among different phases mainly occurs in a relatively low-frequency range. Therefore a three-phase mutual inductance is introduced into the first layer of the RL ladder network of coils, as shown in Fig. 9. Three self-inductances and three coupling factors are required to define a three-phase mutual inductance.

F. Modeling of the Capacitive Coupling Between Winding Coils in the Slot Part

The capacitive coupling in the slot parts must be considered since the distance between conductors belonging to different coils is small, as shown in Fig. 5(a). Therefore, the capacitors corresponding to the thin insulation layer between conductors in the slot part are represented in Fig. 10. The capacitors are marked in different colors because the capacitive coupling from the type 1 coil to the subsequent type 2 coil is not the same as the capacitive coupling from the type 2 coil to the subsequent

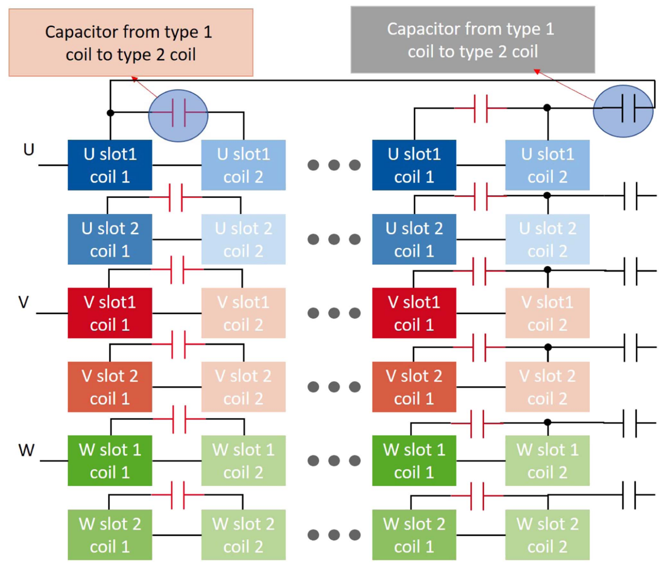

Fig. 10. Capacitive coupling between coils connected in serials in the same phase.

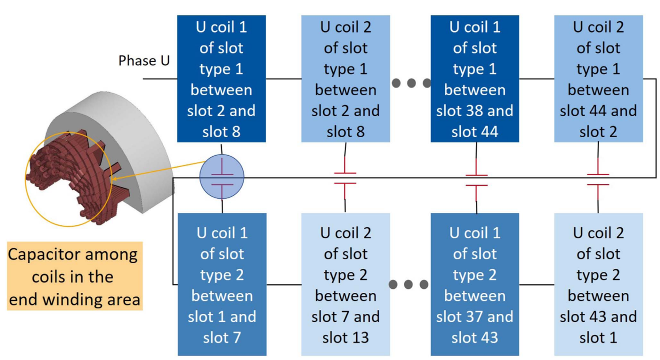

Fig. 11. Capacitive coupling between coils in the end winding area.

type 1 coil due to the variation in the number of contact surfaces between coils.

G. Modeling of the Capacitive Coupling Between Winding Coils in the End Winding Part

Besides the capacitive coupling between conductors in the slot part of electrical machines, the capacitive coupling among conductors in the end winding area must also be considered, as shown in Fig. 11. Furthermore, the location of the capacitive coupling in the end winding area is dependent on the winding connection methods.

IV. Validation of the Coil-Based Model in the Frequency Domain

In order to validate the developed high-frequency models of the PMSM in the frequency domain, the modeled impedance spectra are compared to the measured impedance spectra for various terminal configuration topologies, including phase-to-housing, phase-to-phase, and phase-to-phases. The PMSM's

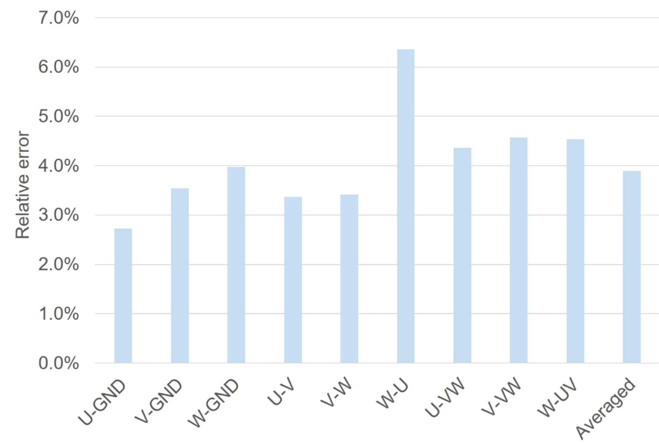

Fig. 12. Diagrammatic comparison of models with different number of mutual inductances regarding the relative deviations Δ_{avg}.

switching frequency during regular operation is approximately 2 kHz. Therefore, the evaluation of impedance spectrum fitting quality is conducted up to 2 MHz, a thousand times the switching frequency. Sufficient high-order harmonics are considered for predicting the voltage distribution along the stator winding.

A total of 145 optimizing parameters are introduced to characterize the entire coil-based grey box model, considering six different slots, each with two different coil types. The parameter fitting process utilizes the differential evolution algorithm described in [22]. In order to quantify the relative variation of the modeled impedance spectra from the measured impedance spectra, an index is defined, as shown in (1)–(2). The parameter Δ_{avg} in (2) represents the average deviation in the modeled impedance spectrum compared to the measured impedance spectra across the frequency range. In the calculation of Δ_{avg}, the n in (2) refers to the number of frequency values at which the impedance is measured. The Δ_{avg} is calculated for different terminal configurations. The parameter $\overline{\Delta}_{\text{averaged}}$, defined in (3), represents the mean value of Δ_{avg} across various measurement topologies. Thereby, the N denotes the total number of impedance measurement topologies considered in the parameter fitting process.

Fig. 12 illustrates the mean errors between the modeled and measured impedance spectra in the frequency range from 1 kHz to 2 MHz. The average deviation between the modeled and measured impedance spectra for all terminal configuration topologies is less than 4 %.

$$\Delta(f_i) = \left| \frac{(|Z_{\text{model}}(f_i)|) - (|Z_{\text{meas}}(f_i)|)}{(|Z_{\text{meas}}(f_i)|)} \right|, \tag{1}$$

$$\Delta_{\text{avg}} = \frac{\sum_{i=1}^{\text{n}} \Delta(f_i)}{n}, \tag{2}$$

$$\overline{\Delta}_{\text{averaged}} = \frac{\sum_{i=1}^{N} \Delta_{\text{avg}}(i - \text{th topology})}{N}, \tag{3}$$

The impedance modeling results obtained using the coil-based grey box model are presented in Figs. 13–15. Specifically, Figs. 14 and 15 display the differential mode impedance spectra, while Fig. 13 represents the common mode impedance spectrum.

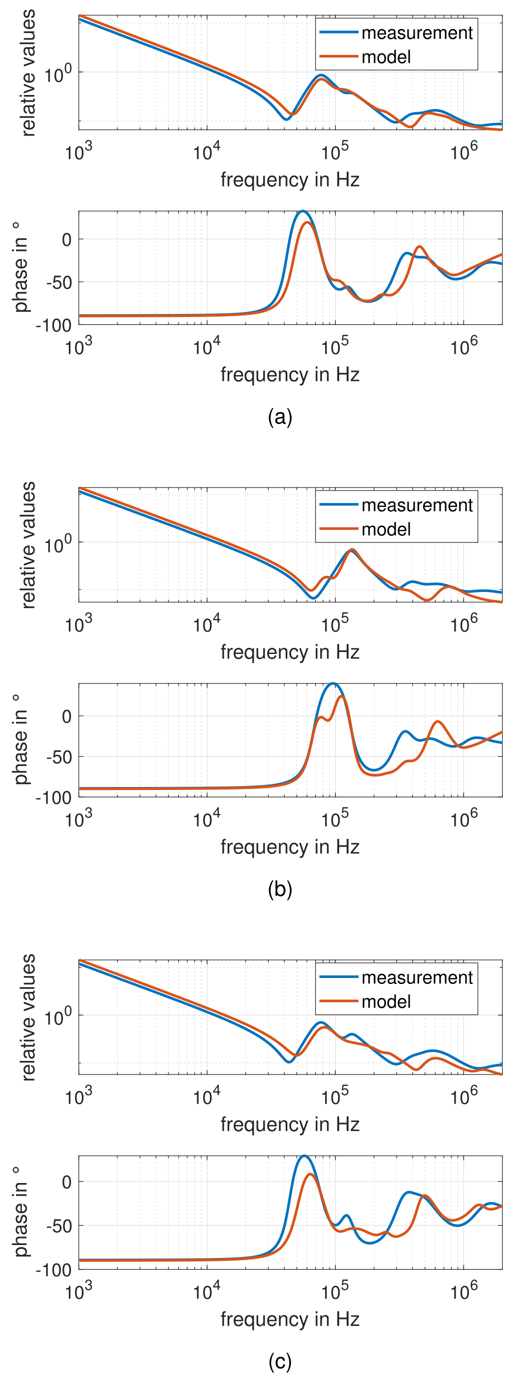

Fig. 13. Validation of phase-housing impedance modeling in frequency domain with comparison to measured values: (a) phase U to housing, (b) phase V to housing, and (c) phase W to housing.

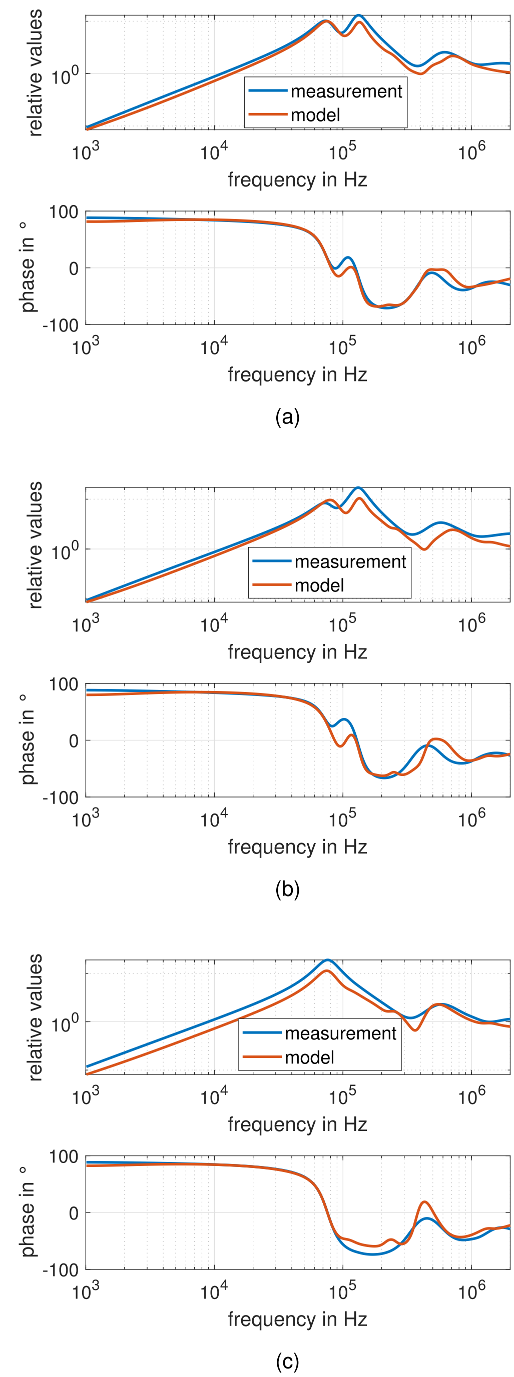

Fig. 14. Validation of phase-phase impedance modeling in frequency domain with comparison to measured values: (a) phase U to V, (b) phase V to W, and (c) phase W to U.

The differential mode impedance spectra, as shown in Figs. 14 and 15, exhibit a high degree of overlap with the measured spectra across a wide frequency range. It indicates the model's accuracy in predicting the differential mode voltage distribution along the stator winding in inverter-fed operations. It is crucial for calculating the maximum voltage in the end winding areas of electrical machines. Furthermore, the modeled phase-to-housing impedance spectra align closely with the measured values, as illustrated in Fig. 13. It implies improved accuracy in modeling the common mode voltage and bearing currents.

The impedance spectra for different rotor positions are also presented in Fig. 16 with the impedance phase U to housing in Fig. 16(a) and phase U to V in Fig. 16(b). It is observed that the impedance spectra for different rotor positions show variation in a low-frequency range below 200 kHz, while they overlap each other in the high-frequency. Since the high-frequency impedance of the machine, including common mode and differential mode,

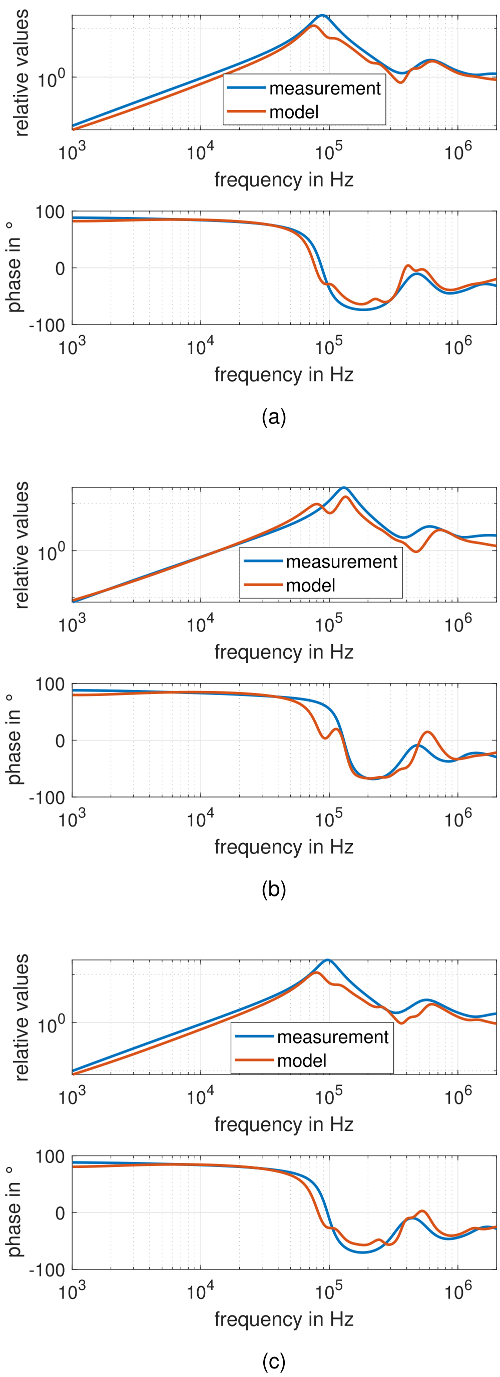

Fig. 15. Validation of phase-two phases impedance modeling in frequency domain with comparison to measured values: (a) phase U to VW, (b) phase V to WU, (c) phase W to UV.

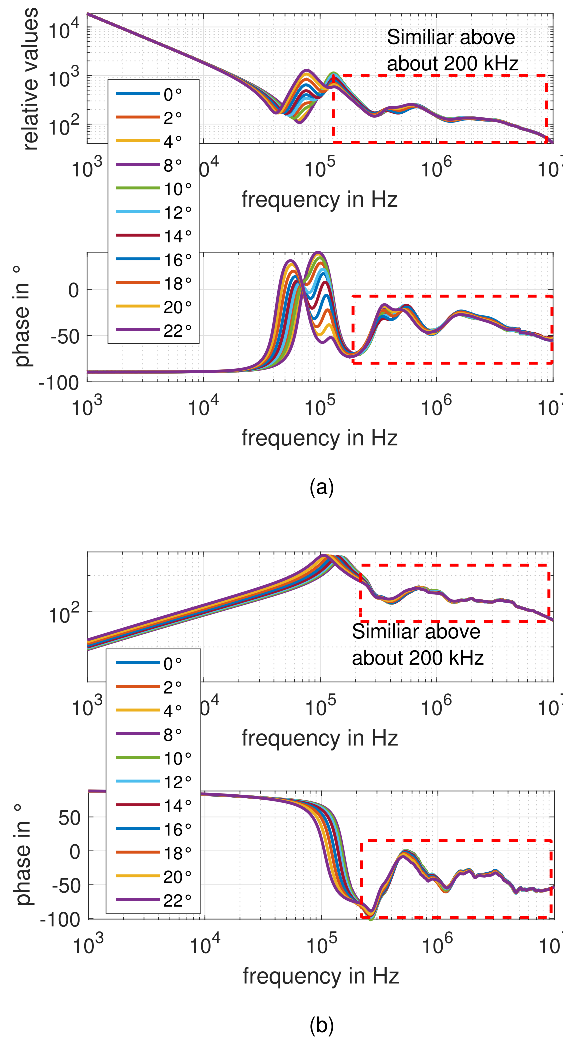

Fig. 16. Measured impedance spectra for a rotor position period from 0° to 22° with a step of 2°: (a) phase U to housing, (b) phase U to VW.

mainly determines the non-uniform voltage distribution along coils and voltage oscillation behavior in electrical machines, the PMSM is firstly parameterized for one rotor position and the model is then used for validation on the test bench in the next section.

In summary, the coil-based grey box model, designed for predicting the voltage distribution along the stator winding of PMSMs, has been validated in the frequency domain. The model captures all primary resonance points below 2 MHz for different typologies. The impact of slight deviations in the phase spectrum on voltage prediction in the time domain will be addressed later. The subsequent section will validate the coil-based model on the test bench using measured voltage signals under various load and rotational speed conditions.

V. Validation of the Coil-Based Grey Box Model in the Time Domain Using Test Bench Measurements

This section will validate the coil-based grey box model through test bench measurements by comparing the modeled voltage signals with their corresponding measured values along the stator winding. In contrast to existing literature, the validation process is performed using an operational PMSM under various load conditions and switching frequencies.

Fig. 17(a) illustrates the electrical circuit configuration of the test bench. The network voltage is rectified to generate a DC-link voltage of 600 V. Power cables are used to connect the inverter and the electrical machine. The shielding of the power

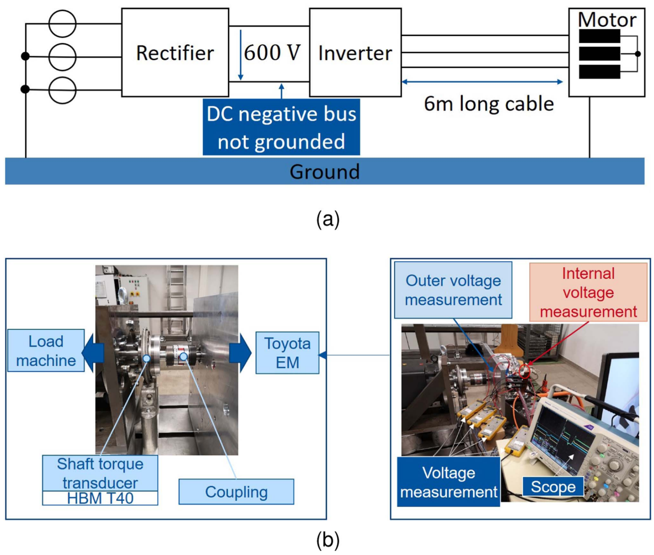

Fig. 17. Test bench: (a) Electrical circuit, (b) voltage measurement configuration during operation of PMSM.

TABLE III
THREE DIFFERENT OPERATIONAL POINTS FOR VALIDATING THE MODEL IN THE TIME DOMAIN

Operation point	Q-axis current	Speed	Switching frequency
1	5 A	500 rpm	2.5 kHz
2	30 A	500 rpm	2.5 kHz
3	30 A	1500 rpm	3.5 kHz

cables and the motor housing are also grounded. Fig. 17(b) presents the actual test bench setup. As mentioned earlier, the winding of the tested PMSM has been modified to enable voltage measurement along the stator winding, as indicated in Fig. 17(b). The distribution of voltage measurement points can be found in Table I. Fig. 17(b) showcases the voltage measurement setups used to validate the modeling of the voltage distribution along the winding. The oscilloscope used in the experiment has four channels with a sampling time of 0.4 ns. Three channels measure the voltage signals between the motor terminals and the housing. In contrast, the fourth channel measures a voltage signal within the electrical machine. Since the available oscilloscope has limited channels, the validation procedure for voltage distribution along the stator winding must be conducted separately.

During the operation of the electrical machine, the DC-link voltage is set at 600 V. The PMSM is operated at three different operating points specified in Table III. The following sections will present the validation results for each operating point for various voltage measurement points listed in Table I.

In the validation process, there are two types of measured voltage profiles: the original signal recorded with a high sampling rate and the one after Fourier processing. The order number for the Fourier processing is set to be 1000 times the switching frequency to reduce computational load. As a result, the measured voltage signal after FFT processing has less noise than the original measured voltage signals. After comparison, the modeled conductor-to-housing voltage signals are overlapped

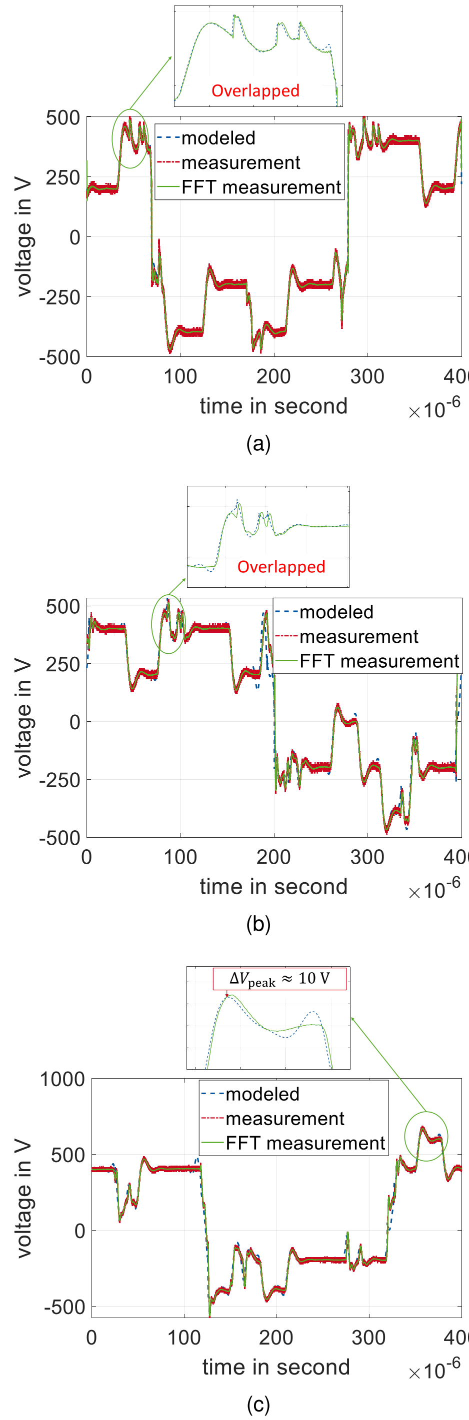

Fig. 18. Comparison of the modeled conductor-housing voltages to measured values at operation point 1: (a) U1e to housing, (b) U7e to housing, and (c) U9e to housing.

with the measured voltage signals for all measuring points within the PMSM, as shown in Fig. 18. Therefore, the voltage peak values between conductors and the stator frame at different welding points can be well predicted. It helps adequately reduce the slot insulation system of electrical machines to improve the heat transfer capability and power density. Besides that, it is observed that the conductor-to-housing voltage does not

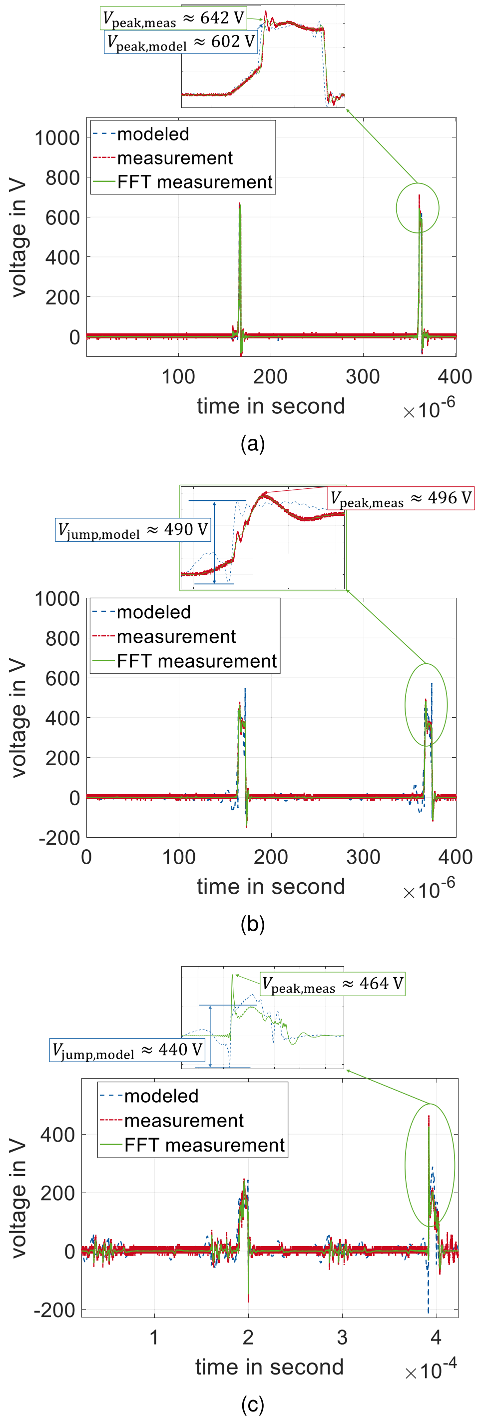

Fig. 19. Comparison of the modeled conductor-conductor voltages to measured values at operation point 1: (a) U1e-V1e with a relative error of 6 %, (b) U7e-V7e with a relative error of 1.2 %, (c) U1e-U8e with a relative error of 5.2 %.

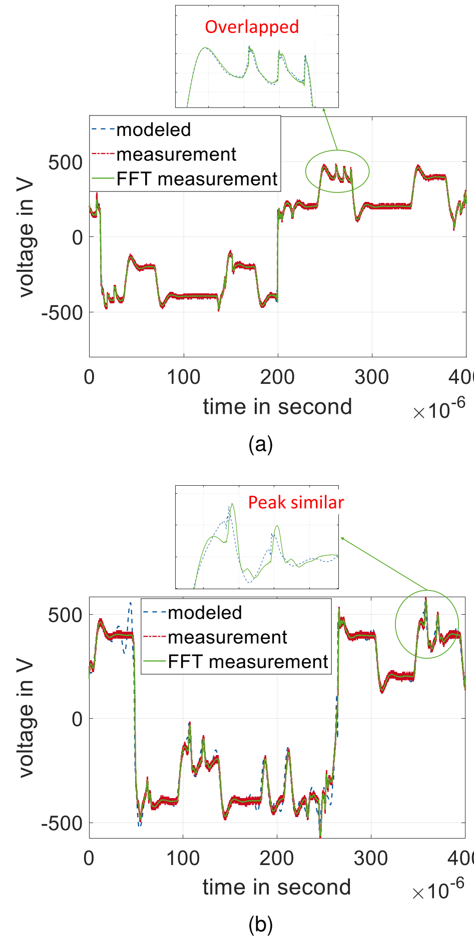

Fig. 20. Comparison of the modeled conductor-housing voltages to measured values at operation point 2: (a) U1e to housing, (b) U7e to housing.

decrease along the stator winding after comparing the maximum voltage voltages at different welding points in Fig. 18.

Fig. 19 compares the modeled and measured conductor-to-conductor voltage profiles at different voltage measurement points. The presented four voltage signals correspond to the most critical cross points among conductors, which suffers from the most extensive electric stress compared to other welding points. It must be mentioned that the location of the cross points with the most significant electric stress depends on the winding configuration and connection typologies. These four cross points are chosen based on the winding typology of the applied PMSM. For the voltage between point U1e and V1e, as shown in Fig. 19(a), the maximum voltage peak and oscillation frequency are overlapped to a large degree between measurement and modeling results.

At other voltage measurement points in Fig. 19(b)–(c), the modeled voltage maximum is less than the measured voltage maximum. One reason lies in the difference in the phase spectra after impedance modeling. The phase difference lies in that merely the impedance spectra's amplitude information is used to define the cost function applied in the optimization program. Therefore, the modeled conductor-conductor voltage show some phase errors. These phase errors are reflected in that the modeled voltage steps down before going up even though the measured signals show purely stepping-up profiles in Fig. 19(b)–(c). Therefore, the evaluation method of the modeled voltage is adjusted to compensate for the phase errors. For this purpose, the voltage jump value instead of the absolute maximum is chosen to be compared to the measured values for welding points. Finally, the relative errors between the modeled and the

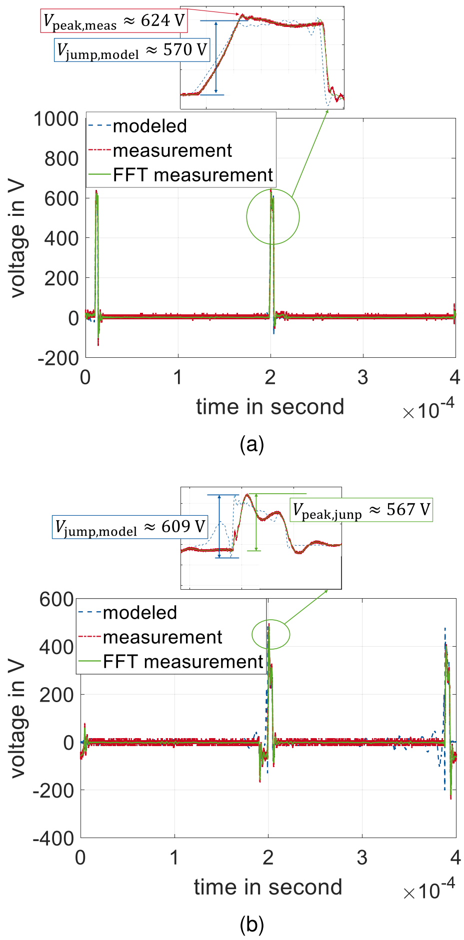

Fig. 21. Comparison of the modeled conductor-conductor voltages to measured values at operation point 2: (a) U1e-V1e with a relative error of 8.7 %, (b) U7e-V7e with a relative error of 7.4 %.

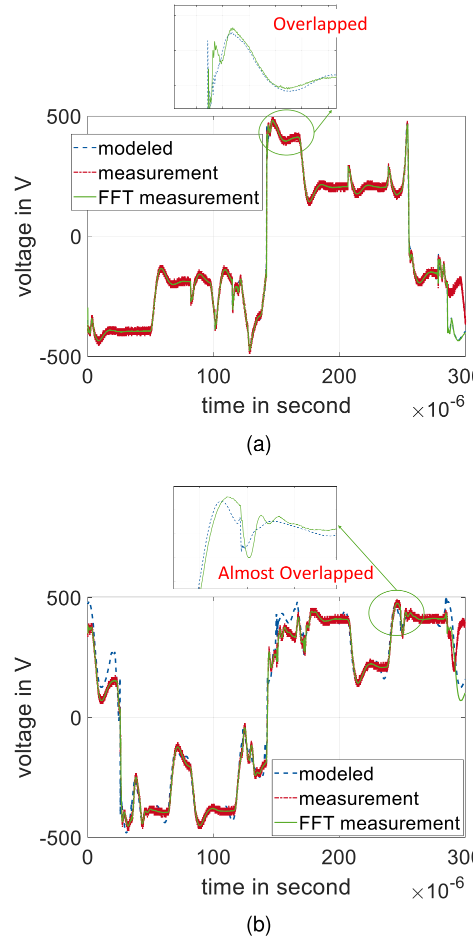

Fig. 22. Comparison of the modeled conductor-housing voltages to measured values at operation point 3: (a) U1e to housing, (b) U7e to housing.

TABLE IV
RELATIVE ERRORS IN THE MODELED CONDUCTOR-CONDUCTOR VOLTAGE SIGNALS FOR DIFFERENT OPERATION POINTS

Error	U1e-V1e	U7e-V7e	U9e-V9e	U1e-U8e
at 1 Operation point	6 %	1.2 %	2.5 %	5.2 %
at 2 Operation point	8.7 %	7.4 %	-	-
at 3 Operation point	4.6 %	1.6 %	-	-

measured signals are calculated and summarized in Table IV, all of which are less than 10 %. It is worth mentioning that the conductor-to-conductor voltage maximum at cross points in the end winding areas decreases toward the neutral point of electrical machines. Therefore, the accuracy in estimating voltage stress at the cross point with the most extensive electric stress is most important, which is the U1e-V1e in our case.

The model validation is also carried out at other operation points. Figs. 20 and 21 shows the results for the working point with a higher q-axis current of 30 A, which helps verify the model accuracy at different load conditions. The modeled conductor-to-housing voltages overlap with the measured values. Besides that, the modeled conductor-to-conductor voltage signals show a maximum relative error of 8.7 % after comparing them to the measured voltage signals. Therefore, it is concluded that the q-axis current does not strongly influence the usability of the coil-based model at different load conditions, even if the model is parameterized by fitting the impedance spectra in no-load states.

Figs. 22 and 23 compare the modeled and measured voltage profiles for the third operation point. The q-axis current here is 30 A, and the rotational speed is 1500 min^{-1} under a switching frequency of 3.5 kHz, which is different from 2.5 kHz before. The modeled conductor-to-housing voltage profiles in Fig. 22 is also similar to the measured voltage profile to a large degree, which verifies the accuracy in modeling common mode voltage at different switching frequencies. The modeled conductor-to-conductor voltage profiles in Fig. 23 show a maximum relative deviation of 7.4 % compared to the measured voltage signals. Therefore, the applicability of the coil-based model for calculating differential mode voltages at different switching frequencies is also validated.

As a summary, the coil-based grey box model, created by fitting impedance spectra measured on the motor's outer accessible terminals, can predict the distribution of the electric potential along stator winding at different operation points. Even though the developed model is fitted using impedance spectra at no-load conditions, the model still works well for different load

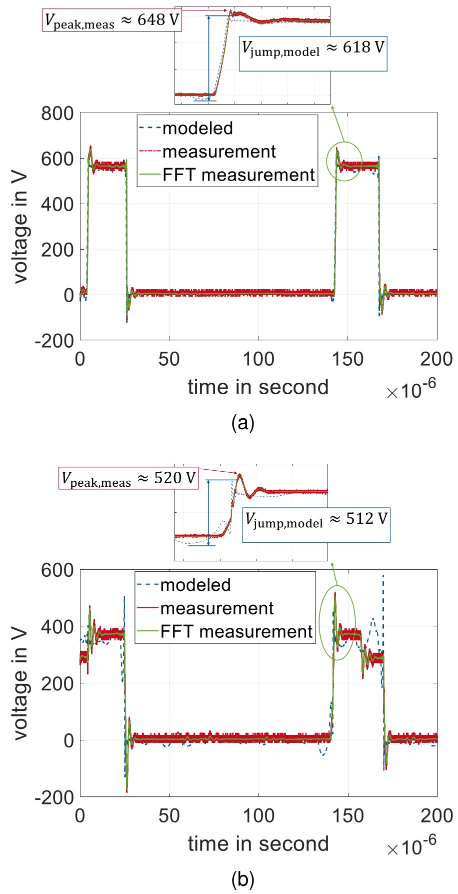

Fig. 23. Comparison of the modeled conductor-conductor voltages to measured values at operation point 3: (a) U1e-V1e with a relative error of 4.6 %, (b) U7e-V7e with a relative error of 1.6 %.

conditions. One possible explanation is that the ferrous materials in the PMSM are saturated due to the interior permanent magnets, and additional current does not enormously change the behaviors of the PMSM in the high-frequency domain. On the other side, even though the used model in the time-domain validation process is parametrized using the impedance measurement for only one rotor position, the model also accurately predicts the voltage distribution during test bench measurement. It has to be mentioned that the rotor position during test bench measurement is not the same as the rotor position for fitting model parameters. The reason is that the high-frequency impedance spectra above 200 kHz are almost the same for all rotor positions, as shown in Fig. 16. Since the high-frequency impedance primarily influences the transient voltage oscillation behaviors in the electrical machines, the maximum voltage values can be predicted without large deviations by using a model fitted by measurement at one rotor position. It reduces the effort for applying the model in practice.

VI. Conclusions and Outlooks

A coil-based grey box model is developed for high-frequency modeling of PMSM with interior magnets in rotors to predict the voltage distribution along stator winding. The coil-based model considers crucial inductive and capacitive coupling in electrical machines' slot and end winding parts. The coil-based model shows an averaged deviation of less than 4 % in the frequency range of from 1 kHz to 2 MHz. Compared to other research, the developed coil-based model enables voltage distribution prediction without creating a white box model using FEM simulations. With the coil-based model's help, the common mode voltage distribution is perfectly predicted with negligible errors between modeled and measured voltage peak values. Regarding the differential mode voltages, they can be predicted with a maximum relative error of less than 10 %, which can help design more suitable insulation thickness of conductors in the next-generation electrical machines. In the future, the phase information can be considered in the parameter fitting process, and the impedance modeling frequency range will be improved to more than 10 MHz for SiC-based electrical drives. Besides that, the coil-based model can also be applied to explore the influence of insulation failure among coils on the outer voltage oscillation behaviors, which may help develop early detection mechanisms for insulation failure.

Acknowledgment

This article is funded by Toyota Motor Corporation. We acknowledge the memory and expresses gratitude to Ms. Isabel Mainz.

References

[1] O. J. Tola, J. G. Ambafi, E. A. Umoh, and O. E. Osinowo, "Performance analysis of a PMSM for traction applications in electric vehicles with hairpin winding technology," in *Proc. IEEE Nigeria 4th Int. Conf. Disruptive Technol. Sustain. Develop.*, 2022, pp. 1–5.

[2] Y. Xie, J. Zhang, F. Leonardi, A. R. Munoz, M. W. Degner, and F. Liang, "Modeling and verification of electrical stress in inverter-driven electric machine windings," *IEEE Trans. Ind. Appl.*, vol. 55, no. 6, pp. 5818–5829, Nov./Dec. 2019.

[3] A. H. Bonnett, "Analysis of the impact of pulse-width modulated inverter voltage waveforms on AC induction motors," *IEEE Trans. Ind. Appl.*, vol. 32, no. 2, pp. 386–392, Mar./Apr. 1996.

[4] G. Almandoz, S. Zarate, A. Egea, Y. Moreno, A. Urdangarin, and R. Moreno, "High frequency modeling of electric drives for electromagnetic compatibility analysis," in *Proc. Int. Conf. Elect. Machines*, 2020, pp. 1129–1135.

[5] M. Ghassemi, "Accelerated insulation aging due to fast, repetitive voltages: A review identifying challenges and future research needs," *IEEE Trans. Dielectr. Electr. Insul.*, vol. 26, no. 5, pp. 1558–1568, Oct. 2019.

[6] H. Zeng, J. Swanke, T. M. Jahns, and B. Sarlioglu, "High-frequency modeling and inter-turn voltage distribution analysis of a modular electric machine for electric aircraft propulsion," in *Proc. IEEE Transp. Electrific. Conf. Expo*, 2022, pp. 1097–1104.

[7] Y. Xu et al., "Impact of high switching speed and high switching frequency of wide-bandgap motor drives on electric machines," *IEEE Access*, vol. 9, pp. 82866–82880, 2021.

[8] A. Hoffmann and B. Ponick, "Method to predict the non-uniform potential distribution in random electrical machine windings under pulse voltage stress," *Energies*, vol. 15, no. 1, 2022, Art. no. 358.

[9] A. Hoffmann and B. Ponick, "Method for the prediction of the potential distribution in electrical machine windings under pulse voltage stress," *IEEE Trans. Energy Convers.*, vol. 36, no. 2, pp. 1180–1187, Jun. 2021.

[10] N. Driendl, F. Pauli, and K. Hameyer, "Characterization of insulation material parameters in low-voltage electrical machines," in *Proc. Int. Conf. Elect. Machines*, 2022, pp. 1314–1320.

[11] *Rotating Electrical Machines—Part 18-41: Partial Discharge Free Electrical Insulation Systems (type I) Used in Rotating Electrical Machines Fed From Voltage Converters—Qualification and Quality Control Tests*, International Standard, I. 60034-18-41,Geneva, Switzerland, 2014.

[12] J. Dittmann, M. England, and B. Ponick, "Design of hairpin windings considering the transient potential distribution," *e i Elektrotechnik und Informationstechnik*, vol. 140, no. 2, pp. 271–280, 2023.

[13] M. S. Toulabi, L. Wang, L. Bieber, S. Filizadeh, and J. Jatskevich, "A universal high-frequency induction machine model and characterization method for arbitrary stator winding connections," *IEEE Trans. Energy Convers.*, vol. 34, no. 3, pp. 1164–1177, Sep. 2019.

[14] Y. Wu et al., "High-frequency modelling of permanent magnet synchronous motor with star connection," *IET Electric Power Appl.*, vol. 12, no. 4, pp. 539–546, 2018.

[15] B. Heidler, K. Brune, and M. Doppelbauer, "High-frequency model and parameter identification of electrical machines using numerical simulations," in *Proc. IEEE Int. Electric Machines Drives Conf.*, 2015, pp. 1221–1227.

[16] Y. Xie, J. Zhang, F. Leonardi, A. R. Munoz, and M. W. Degner, "Investigation of surge voltage propagation in inverter-driven electric machine windings," *IEEE Trans. Ind. Electron.*, vol. 70, no. 10, pp. 9811–9822, Oct. 2023.

[17] O. Magdun, S. Blatt, and A. Binder, "Calculation of stator winding parameters to predict the voltage distributions in inverter fed ac machines," in *Proc. 9th IEEE Int. Symp. Diagnostics Electric Machines, Power Electron. Drives*, 2013, pp. 447–453.

[18] O. Magdun and A. Binder, "High-frequency induction machine modeling for common mode current and bearing voltage calculation," *IEEE Trans. Ind. Appl.*, vol. 50, no. 3, pp. 1780–1790, May/Jun. 2014.

[19] D. A. Hewitt, S. Sundeep, J. Wang, and A. Griffo, "High frequency modelling of electric machines using finite element analysis derived data," *IEEE Trans. Ind. Electron.*, vol. 71, no. 2, pp. 1432–1442, Feb. 2024.

[20] S. Sundeep, J. Wang, and A. Griffo, "Holistic modeling of high-frequency behavior of inverter-fed machine winding, considering mutual couplings in time domain," *IEEE Trans. Ind. Appl.*, vol. 57, no. 6, pp. 6044–6057, Nov./Dec. 2021.

[21] J. E. Ruiz-Sarrio, F. Chauvicourt, J. Gyselinck, and C. Martis, "Impedance modeling oriented toward the early prediction of high-frequency response for permanent magnet synchronous machines," *IEEE Trans. Ind. Electron.*, vol. 70, no. 5, pp. 4548–4557, May 2023.

[22] Y. Zhang, H. Peng, and W. Hofmann, "Transient skin effect in highly dynamic induction motor drives: Energy-optimized design," *Elect. Eng.*, vol. 105, pp. 1015–1024, 2023.

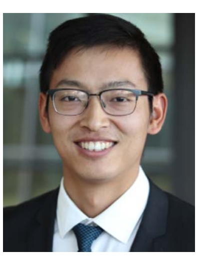

Hujun Peng received the bachelor's degree in electrical engineering from Zhejiang University, Hangzhou, China, in 2013, the master's degree in electrical engineering from the Dresden University of Technology, Dresden, Germany, in 2017, and the Ph.D. degree from RWTH Aachen University, Aachen, Germany, in 2023. Since 2018, he has been a Research Assistant with the Institute of Electrical Machines, RWTH Aachen University. Since then, he has been a Postdoctoral Researcher with the Institute of Electrical Machines. His research interests include high-frequency modeling of electrical machines, energy management of fuel cell hybrid vehicles, characterization of insulation systems in electric machines and the analysis of parasitic effects in electric drives.

Svetomir Stevic (Graduate Student Member, IEEE) received the Diploma from the School of Electrical Engineering, University of Belgrade, Belgrade, Serbia, in 2011, and the M.Sc. in electrical engineering from RWTH Aachen University, Aachen, Germany, in 2016. From 2016 to 2018 he was with the Idaho National Laboratory, Idaho Falls, ID, USA, on topics including design, modeling and simulation of power converters, energy devices and power grids as well as controller- und power-hardware-in-the-loop tests for intelligent power grids. Since August 2018, he has been with the Institute of Electrical Machines, RWTH Aachen University, on topics including co-design, prototyping and control of power electronics and electrical machines as well as analysis of interaction mechanisms in electrical drives.

Ze Luo received the bachelor's degree in electrical engineering and information technology in March 2023 from RWTH Aachen University, Aachen, Germany, where he is currently working toward the Master of Science degree in systems and automation. Since 2023, he has been a Student Assistant with the Institute of Electrical Machines, RWTH Aachen University. His research interests include high-frequency modeling of electrical machines.

Niklas Driendl received the M.Sc. degree in electrical engineering from RWTH Aachen University, Aachen, Germany, in 2018. In 2019, he joined the Institute of Electrical Machines, RWTH Aachen University, as a Research Associate. His research interests include characterization of insulation systems of electrical machines, modeling of partial discharge processes and analysis of aging processes.

Daniel Butterweck received the M.Sc. degree in electrical engineering from RWTH Aachen University, Aachen, Germany, in 2013. Since 2014, he has been a Research Associate with the Institute of Electrical Machines (IEM), RWTH Aachen University. There, he led the "Automotive" Research Group from 2017 to 2018. Since 2018, he has been a Chief Engineer with IEM. His research focuses on the design and simulation of electrical drivetrains and machines.

Leila Sharifian received the master's degree from the Sharif University of Technology, Tehran, Iran, in 2004, and the doctor's degree in mechanical and process engineering from the Swiss Federal Institute of Technology Zurich, Switzerland, in 2011. After that, she was a Postdoctoral Researcher. Since 2012, she has been with Toyota Motor Europe. She is currently a Technical Manager in powertrain digital, E-motor pre-development, and BEV thermal management system improvement. Her research interests include electric motors, gasoline engines, battery & system thermal management, and diesel engines.

Yousef Firouz received the Doctoral degree in engineering sciences with a thesis entitled“Advanced system identification and modeling of lithium-ion batteries in the time and frequency domains” from Vrije Universiteit Brussel, Belgium, in 2019. He is currently a Research Engineer with Toyota Motor Europe. His fields of expertise include characterization, electrothermal and electrochemical modelling of Li-ion batteries, high frequency electric machine modeling, and power electronics.

Kay Hameyer (Senior Member, IEEE) received the M.Sc. degree in electrical engineering from the University of Hannover, Hanover, Germany, and the Ph.D. degree from the University of Technology Berlin, Berlin, Germany, in 1986 and 1992, respectively, for working on permanent magnet excited machines. After his university studies, he was with the Robert Bosch GmbH, Stuttgart, Germany, as a Design Engineer for permanent magnet servo motors. From 1988 to 1993, he was a Member of Staff with the University of Technology Berlin, Berlin, Germany. From 1996 to 2004, he was then a Full Professor of numerical field computations and electrical machines with Katholieke Universiteit Leuven (KU Leuven), Leuven, Belgium. Since 2004, he has been a Full Professor and the Director of the Institute of Electrical Machines (IEM), RWTH Aachen University, Aachen, Germany. The characterization and modeling of hard- and soft-magnetic materials is another focus of his work. He has authored/coauthored more than 350 journal publications, more than 700 international conference publications and four books. His research interest focuses on all aspects of the design, control and manufacturing of electrical machines and the associated numerical simulation. His research interests include numerical field computation and optimization, the design and control of electrical machines, in particular, permanentmagnet excited machines, induction machines. Dr. Hameyer is a Member of the German VDE and a Fellow of the Institution of Engineering and Technology, U.K.